Toxicology Research

PAPER

View Article Online
View Journal | View Issue

Cite this: *Toxicol. Res.*, 2016, **5**, 248

Toxicity mechanism in fetal lung fibroblast cells for multi-walled carbon nanotubes defined by chemical impurities and dispersibility†

Aparna Shinde[a] and Candace S. J. Tsai*[a,b]

Multi-walled carbon nanotubes (MWCNTs) are beneficial in a wide range of applications in fields such as electronics, optics and nano-medicine, so knowledge concerning their effect on human health is important. Physiochemical properties of MWCNTs can greatly affect their toxicity, however, there are no reports discussing the effect of size and chemical composition of MWCNTs on the toxic response of human lung cells. In this study, MWCNTs of two different purity grades were characterized and their toxic effects were compared on normal fetal lung fibroblast MRC-5 cells. The toxic effect on MRC-5 cells following 1–3 days exposure to low concentrations of research grade (RG) and industrial grade (IG) MWCNTs were studied using multiple biological assays. MWCNTs uptake in MRC-5 cells was analyzed using TEM. After physical and chemical analysis, RG-MWCNTs revealed contamination with MoS_2 and were readily suspended in distilled water while IG-MWCNTs had no MoS_2 contamination and much lower dispersibility. For a wide range of concentrations and exposure times, cells treated with RG-MWCNTs had distinctly reduced cell viability as compared to cells treated with IG-MWCNTs. Treatment with RG-MWCNTs resulted in high reactive oxygen/nitrogen species (ROS/RNS) levels indicating an oxidative stress mechanism while IG-MWCNT treated cells had low ROS/RNS amounts and a distorted cell membrane pointing towards a non-oxidative stress mechanism. Both agglomerates and individual MWCNTs were internalized efficiently by MRC-5 cells, which resulted in cell damage and ultimately cell death. Altogether, this study shows that the MoS_2 contamination and size of MWCNTs' agglomerates affect the mechanism of toxicity in human fetal lung fibroblasts.

Received 28th June 2015,
Accepted 25th October 2015

DOI: 10.1039/c5tx00211g

www.rsc.org/toxicology

Introduction

Since the early 1990s, engineered nanomaterials (ENMs) have been discovered and applied to the development of the nanotechnology industry;[1] this development has led to concerns about possible human exposure and resulting adverse health effects. Currently, the effects from exposure to various kinds of ENMs are not well understood. The carbon nanotube (CNT), discovered in 1991, is one of the most widely used ENMs and is manufactured globally at a very large scale; both humans and the environment thus have increased chances for exposure. The global production of MWCNTs has increased from 3100 to 6900 tons per year from 2010 to 2014.[2–4] CNTs have received increasing interest in research and industry due to their unique properties arising from their cylindrical structure.[1,5] CNTs, in particular multi-walled CNTs (MWCNTs), are finding wide applications in electronics, medicine, optics and other fields of materials sciences.[6–8] Even though MWCNTs are extremely useful and promising in different areas of industrial and biomedical research, there are conflicting data regarding health hazards associated with CNT exposure.

Owing to their nanometer size and high surface to volume ratio, CNTs can extensively interact with cells and activate a cascade of biological processes such as reactive oxygen/nitrogen species production, causing DNA damage and cell death through apoptosis and necrosis.[9,10] This response is possible for small MWCNTs that can efficiently enter the cells. MWCNTs have potential to cause genotoxicity through non-oxidative stress, extensive membrane damage and apoptosis.[11] Individuals can be exposed either to individual MWCNTs or to

[a]*Birck Nanotechnology Center, Discovery Park, Purdue University, 1205 West State Street, West Lafayette, IN 47907, USA*
[b]*Department of Environmental and Radiological Health Science, Colorado State University, 1681 Campus Delivery, Fort Collins, CO 80523-1681, USA.*
E-mail: Candace.Tsai@colostate.edu; Tel: +1 (970) 491-1340

†Electronic supplementary information (ESI) available: Characterization of MWCNTs for elemental composition using TEM EDX, size distribution using Nanosight and XPS spectra of C 1s and O 1s for IG-MWCNTs and RG-MWCNTs (Fig. S1, S2 and Table 1). See DOI: 10.1039/c5tx00211g

MWCNT agglomerates in an industrial or lab setting. The mechanism for inducing toxicity for larger agglomerates could be different from that for individual MWCNTs, and may be through non-oxidative processes and cell membrane damage. Thus, MWCNTs can induce toxicity through both oxidative and non-oxidative processes. However, the factors that cause the differences in toxicity mechanisms exhibited by different sizes of MWCNTs have not been studied. *In vitro* studies have found that CNTs can cause cytotoxicity in different cell lines, including RAW 264.7 macrophages, rat macrophages (NR8383), human embryo kidney cells (HEK293) and human dermis fibroblasts.[12–15] Furthermore, Meng *et al.* have found MWCNTs to affect the blood coagulation process through extensive erythrocyte damage, platelet activation and reduction of platelet viability.[16]

The toxicity exhibited by MWCNTs is attributed to their physical and chemical properties. Researchers have proposed that the toxic effect of CNTs varies with their size, surface chemistry, tube length and composition. However, there is a significant knowledge gap concerning whether elemental composition affects the agglomerate size of MWCNTs. Several studies have investigated modification of the surface chemistry (functionalization) to study the size effect in a solvent,[17,18] which does not simulate living tissue exposure. In one study with living tissue, MWCNTs tended to agglomerate and form large agglomerates due to their discrete geometric shape.[19] In another study, MWCNTs were uniformly dispersed and caused significant developmental defects in zebrafish.[20] There is no consistent data concerning the dispersion and size distribution of MWCNTs and the toxic effects induced in human lung cells.

Studies investigating the effect of CNTs on human lung cells are important because of the likelihood of exposure to airborne CNTs through inhalation. However, there is still ongoing debate concerning how MWCNTs' size affects cellular mechanisms and hinders the normal cellular processes leading to toxicity in human lung cells. Little information is available regarding whether large agglomerates of MWCNTs or smaller individual nanotubes induce greater toxic effects, and the mechanisms associated with those effects. There is no conclusive study to date that compares the toxicity exhibited by MWCNTs that have similar manufacturing processes but vary in chemical composition and the quantity and physical states of metal impurities. In this study, we investigated the effect of chemical composition and size of MWCNTs' agglomerates on the cellular response.

Given these facts and the uses of these novel ENMs in various fields, it is important to evaluate the adverse effects of MWCNTs in normal lung cells with respect to exposure duration, concentration, fiber length/size and elemental composition. This research article focuses primarily on the difference in the cellular response and cytotoxicity level of normal lung cells following exposure to different MWCNTs. In addition, characterization of two purity grades of MWCNTs was performed to correlate the difference in cell response following exposure to the CNT properties.

Materials and methods

Characterization of MWCNTs

Two different MWCNTs, industrial grade (IG) and research grade (RG) were purchased from Nanolab Inc. (179 Bear Hill Rd # 8, Waltham, MA 02451, USA). Both IG-MWCNTs and RG-MWCNTs are produced using chemical vapor deposition. Analyses performed in this study were for the purchased material, and may not be representative for this grade of product. For size and structure analysis using transmission electron microscopy (TEM), 1 mg ml^{-1} samples of MWCNTs were prepared in distilled water, and sonicated for 10 minutes and diluted 100 times to obtain a uniform dispersion of 10 μg ml^{-1}. MWCNT suspensions were then dispersed on glow discharged 400 mesh copper TEM grids coated with 10 nm formvar and 3–4 nm carbon purchased from Electron Microscopy Sciences so that hydrophobic MWCNTs were collected on the grid for imaging. A FEI Technai G2 20 TEM equipped with an Oxford INCA 250 X-MAX 80 silicon drift electron dispersive X-ray analysis (EDX) system was operated at 200 kV to perform image and elemental composition analysis. Samples were characterized for elemental composition using the Kratos X-ray Photoelectron Spectroscopy (XPS) facilities at Birck Nanotechnology Center at Purdue University. Curve fitting for XPS spectra was done using Origin software. For size distribution analysis, MWCNTs were suspended in distilled water at a concentration of 1 μg ml^{-1}, sonicated for 10 min and analyzed using the Malvern Nanosight LM10 instrument. This unique technology utilizes the properties of both light scattering and Brownian motion in order to obtain the size distribution and concentration measurement of particles in liquid suspension with real-time response each second.

Cell culture

For *in vitro* studies, human fetal lung fibroblast (MRC-5) cells were purchased from American Type Culture collection (ATCC). MRC-5 cells were cultured in ATCC formulated Eagles Minimum Essential Media supplemented with 10% fetal bovine serum, 1% penicillin and streptomycin under 5% CO_2 atmosphere at 37 °C. The cells were passaged for 2 weeks prior exposure to MWCNTs.

Calcein AM assay

MRC-5 cell viability was assessed following incubation with MWCNTs using the calcein AM assay kit from Trevigen™. Cells were seeded in 96 well plates at a density of 10 000 cells per well and incubated for 24 h, after which the cells were exposed to IG-MWCNTs or RG-MWCNTs suspended in distilled water at concentrations of 1 μg ml^{-1}, 5 μg ml^{-1}, 10 μg ml^{-1} and 20 μg ml^{-1} for 24, 48 and 72 h. The cells were washed with PBS and 100 μl buffer provided with the calcein AM cell viability kit and incubated with 1 μM calcein AM for 30 min. Cells incubated in pure cell culture medium were used as negative controls. The fluorescence was measured at 485/520 nm using a fluorescence plate reader. Live or viable cells exhibit fluorescence, which is measured as relative

fluorescence units (RFU). RFU values were normalized to % cell viability with respect to 100% cell viability for cells non-exposed to MWCNTs.

Total ROS/RNS assay

We analyzed total ROS/RNS species *in vitro* using the ROS/RNS detection kit for microscopy from Enzo™ life sciences and Oxi-Select™. Cells were seeded in 24 well plates at a density of 50 000 cells per well and incubated for 24 h, after which the cells were exposed to a concentration of 1 μg ml^{-1}–20 μg ml^{-1} of MWCNTs (IG or RG) for 24 h. Following incubation, the ROS/RNS were detected using non-fluorescent agents provided in the kit using the established protocol. For ROS and nitric oxide (NO) radical negative controls, cells were treated with ROS inhibitors and NO radical scavengers for 30 minutes respectively. For positive control, cells were treated with ROS and NO inducers. Following staining, images were obtained using an Olympus FV1000 confocal microscope. Oxidative stress was determined using a total ROS detection dye (FITC green) that uniformly stained cell cytoplasm. The total ROS dye reacts with hydrogen peroxide (H_2O_2), peroxynitrite ($ONOO^-$) and hydroxyl radicals. Superoxide radicals were detected using Rhodamine red stain that specifically stained superoxide radicals in the nucleus. Cyanine 5 was used to detect NO species, which occurred as punctuate staining throughout the cytoplasm. We didn't have a filter set (650 nm/670 nm) compatible with Cyanine 5 and therefore we false colored the grey images of NO radicals with a yellow color using Image J. ROS/RNS quantity in MRC-5 was determined using the OxiSelect™ *in vitro* ROS/RNS assay kit. The cells were washed with PBS and incubated with 2′,7′-dichlorodihydrofluorescein dye for 15–45 minutes. Following incubation, the cells were measured for 2′,7′-dichlorofluorescein (DCF) fluorescence using a fluorescence plate reader. Cells incubated in pure cell culture medium were used as negative controls.

Hoechst 33342 assay

Apoptotic phenotype of MRC-5 cell was determined following incubation with MWCNTs using a Hoechst 33342 dye. Cells were seeded in 24 well plates at a density of 50 000 cells per well and incubated for 24 h, after which the cells were exposed to a concentration of 1 μg ml^{-1}–20 μg ml^{-1} of MWCNTs (IG or RG) for 24 h. The cells were washed with PBS and stained with 1 μM Hoechst dye for 10–15 min. Following staining, the cells were imaged for apoptotic nuclei under a fluorescence microscope using UV filters and changes in cell shape and membrane structure were evaluated using phase contrast. Cells incubated in pure cell culture medium were used as negative controls.

Annexin V assay

Apoptosis was determined following incubation with MWCNTs using Annexin V dye. Cells were seeded in 24 well plates at a density of 50 000 cells per well and incubated for 24 h, after which the cells were exposed to a concentration of 1 μg ml^{-1}–20 μg ml^{-1} of MWCNTs (IG or RG) for 24 h. The cells were washed with PBS and stained with 5 μl of Annexin V for 15 min. Following incubation, the cells were analyzed for apoptosis using the Annexin V FITC kit from Cayman. The fluorescence was detected using a fluorescence plate reader. Cells incubated in pure cell culture medium were used as negative controls.

Imaging carbon nanotubes in cells using TEM

Cells were seeded in 60 mm tissue culture plates at a density of 10^5 cells per plate and incubated for 24 h, after which the cells were exposed to a concentration of 5 μg ml^{-1} of MWCNTs (IG or RG) for 24 h. The cells were then harvested and washed twice with PBS. Cultured cells were fixed in 2.5% glutaraldehyde in 0.1 M cacodylate buffer (pH 7.4), post-fixed in 1% OsO_4 in 0.1 M cacodylate buffer, de-hydrated in ethanol, and embedded in epoxy resin. Ultrathin sections were contrasted in lead-hydroxide, studied and photographed by a CM100 Transmission Electron Microscope. Transmission electron microscopy analyses were performed in three independent experiments. Three ultrathin sections were analyzed for each sample in each experiment.

Statistical analysis

The number of live cells were calculated as a percentage of the number of controls (100%) in the same experiment and shown as mean ± SEM (standard error of the mean) of at least 3 independent experiments with consecutive passages. We used one way analysis of variance (ANOVA) on JMP 11 for statistical comparisons between the concentrations of each MWCNTs and multiple ANOVA for comparisons between multiple factors. At 95% confidence level, p values <0.05 were considered statistically significant.

Results

Characterization of MWCNTs

Transmission electron microscopy (TEM) analysis. MWCNTs were studied for fiber size and structure using TEM. The micrographs shown in Fig. 1 display the structure of IG-MWCNTs (Fig. 1a) and RG-MWCNTs (Fig. 1b) suspended in distilled water post 10 min sonication (Fig. 1c). The diameter of IG-MWCNTs was approximately 10 nm (Fig. S1a†) and the diameter for RG-MWCNTs was approximately 15 nm (Fig. S1b†). IG-MWCNTs formed agglomerates in which the fibers were entangled with very few fibers protruding from the agglomerate (Fig. 1a and S1c†). In contrast, RG-MWCNTs formed large agglomerates in which, even though entangled, the fibers extended extensively from the agglomerates and had a compact arrangement (Fig. S1d†). Following sonication, RG-MWCNT agglomerates were broken into individual smaller/shorter nanotubes as short as 100 nm as shown in Fig. 1b. In addition, significant differences were observed between the two materials in elemental composition and solubility properties. Energy Dispersive X-ray spectroscopy (EDX) analysis with TEM was used to determine elemental composition.

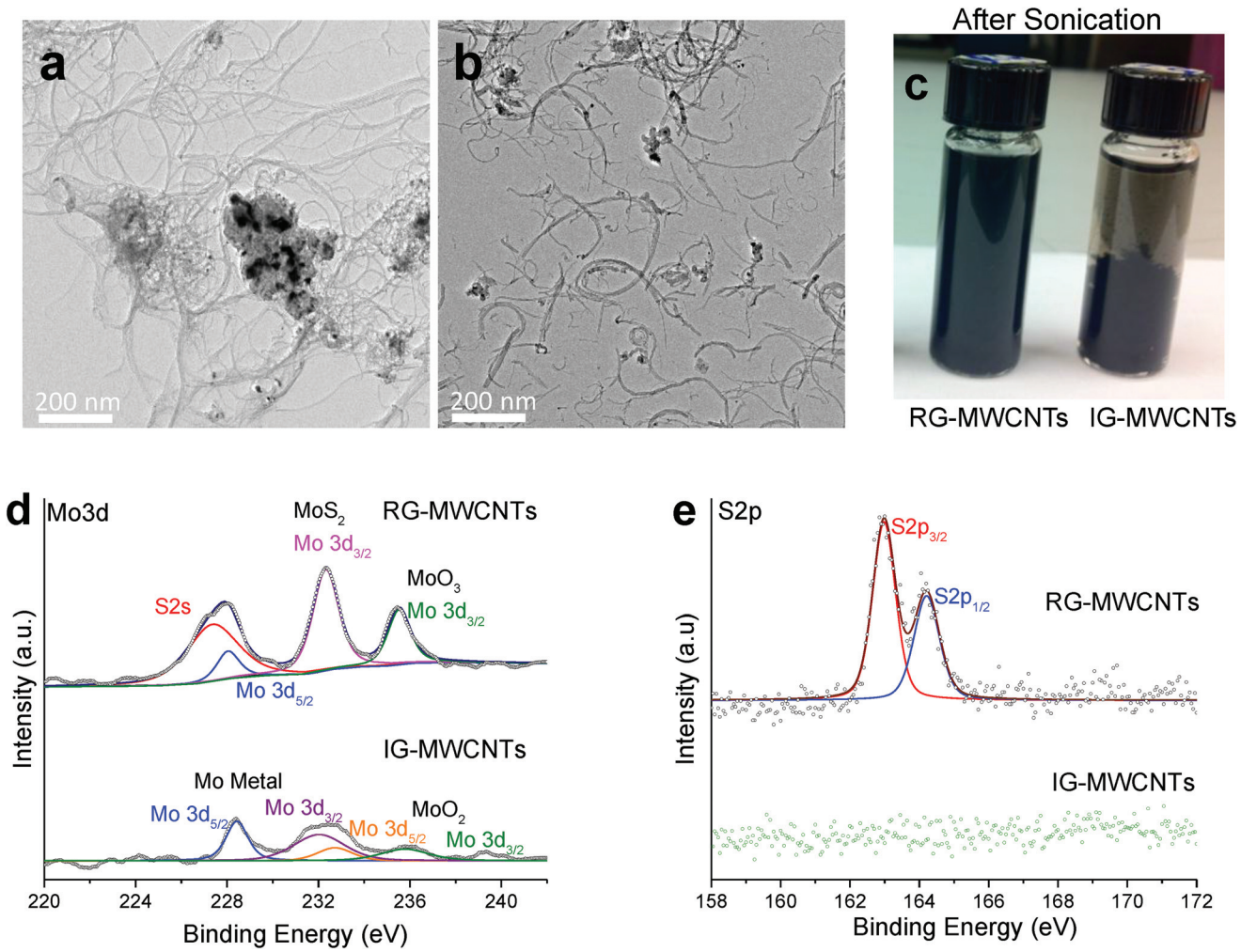

Fig. 1 Characterization of MWCNTs. (a) Transmission electron micrographs (TEM) of IG-MWCNTs and (b) and RG-MWCNTs. (c) Post sonication images of 1 mg ml^{-1} MWCNTs (IG and RG) showing markedly different dispersibility in di water. Comparative XPS spectra for IG-MWCNTs and RG-MWCNTs of (d) Mo 3d and (e) S 2p. Note the differing chemical states of Mo present in the two types of MWCNTs. In addition, RG-MWCNTs show S 2p peaks from MoS_2 while IG-MWCNTs are completely devoid of MoS_2.

The TEM EDX spectrum of IG-MWCNTs displayed carbon, oxygen and molybdenum (Fig. S1e†) whereas RG-MWCNT agglomerates (Fig. S1f†) revealed the presence of carbon, oxygen, molybdenum and sulfur. Sulfur was found to be absent in IG-MWCNT agglomerates. The percentage of chemical composition along with impurities are listed in Table S1† for both IG-MWCNTs and RG-MWCNTs. IG-MWCNTs contain high percentage of O and Mo as impurities compared to RG-MWCNTs, which predominantly contained O, Mo and S impurities. The difference in the trace impurities of MWCNTs along with their surface properties may affect their dispersity and agglomerate size in water. The two MWCNTs behaved differently in terms of dispersibility. During sonication, RG-MWCNTs broke into nanometer-size fibers and formed a uniform dispersive solution whereas sonication had no effect on the dispersion of IG-MWCNTs and therefore IG-MWCNTs had bigger agglomerates as compared to RG-MWCNTs. Fig. S1g† and 1c illustrate the dispersion of IG-MWCNTs and RG-MWCNTs in distilled water before sonication and after sonication respectively. The size distributions of both IG-MWCNTs and RG-MWCNTs in distilled water were determined with Malvern NanoSight LM10 utilizing Nanoparticle Tracking Analysis (NTA) technology. The concentration of nanometer-sized particles in distilled water was found to be zero. The average agglomerate sizes of RG-MWCNTs and IG-MWCNTs are 129 nm and 291 nm, respectively (Fig. S1h†). The mobility size of RG-MWCNTs and IG-MWCNTs varies between 50–700 nm and 600–1000 nm in distilled water (Fig. S1h†), respectively. Both have diameters between 5–20 nm according to TEM (Fig. S1a and S1b†). The above data suggest the presence of a mixture of individual MWCNTs and agglomerated MWCNTs for both RG-MWCNTs and IG-MWCNTs. The Nanosight results suggest that RG-MWCNTs had a higher portion of nanometer-sized fibers (<150 nm)

than IG-MWCNTs. From the above characterization results, we concluded that there is a difference in the size distribution and dispersibility in distilled water between the two types of MWCNTs.

X-ray photoelectron spectroscopy (XPS). XPS analysis was performed to confirm the difference in the elemental composition of the two types of MWCNTs. Fig. 1d and e display the comparative XPS spectrum of molybdenum disulfide (Mo 3d and S 2s) between IG-MWCNTs and RG-MWCNTs. Four elements were detected by XPS analysis for RG-MWCNTs, which included molybdenum, sulfur, carbon, and oxygen (Fig. 1d, e, S2a and S2b†). In contrast, sulfur was absent in IG-MWCNTs as confirmed by the missing sulfur peak. In the molybdenum peak of IG-MWCNTs, four peaks visible at 228.1, 231.5, 232.2 and 235.8 eV were detected and could be assigned to Mo and MoO_2 (Fig. 1d). The molybdenum XPS scan for RG-MWCNTs displayed two MoS_2 characteristic peaks at 232.5 and 226.7.3 eV, which were associated with S 2s (Fig. 1d). The XPS scan of the sulfur region displayed the two typical peaks at 162.6 and 164.2 eV that could be assigned to S $2p_{3/2}$ and S $2p_{1/2}$, respectively (Fig. 2e). The MoS_2 peaks were absent in IG-MWCNT's XPS scan, which is consistent with the absence of peaks in the sulfur region. The comparative XPS spectra of C 1s and O 1s between IG-MWCNTs and RG-MWCNTs are shown in Fig. S2.† The C 1s core peak levels of carbon atoms for both IG-MWCNTs and RG-MWCNTs were observed at approximately 284.5 eV (Fig. S2a†). Oxygen binding energy O 1s was deconvulated into two peaks at 532.3 and ~532.8 eV, which could be labeled as C–OH and C═O respectively (Fig. S2b†). Thus, the above data suggested that IG-MWCNTs contained some oxygen and trace amounts of molybdenum impurities, whereas RG-MWCNTs predominantly contained MoS_2, trace amounts of Mo metal and Mo oxide impurities.

Cytotoxicity in normal lung cells

Cell viability of normal lung cells. As displayed in Fig. 2, with increase in concentration of IG-MWCNTs or RG-MWCNTs and exposure duration (24–72 h), there was significant reduction in cell viability of the fetal lung fibroblasts cells (MRC-5). After 24 h incubation, 1 μg ml^{-1} of RG-MWCNTs caused 30% less cell viability in normal cells compared to 1 μg ml^{-1} of IG-MWCNTs. Moreover, we noted different toxicity effects of IG-MWCNTs and RG-MWCNTs on MRC-5 cells as shown in Fig. 2a and b. Furthermore, the fraction of live cells decreased with the increase in concentration of either IG-MWCNTs or RG-MWCNTs after 24 h treatment and the lowest cell viability of less than 50% was detected at a concentration of 20 μg ml^{-1} for both IG-MWCNTs and RG-MWCNTs. After treatment for 48 h and 72 h, similar toxicity was noticed at a concentration of 1 μg ml^{-1} but a significant toxicity difference was discerned at higher concentrations. RG-MWCNTs instigated 75% cell death at concentrations higher than 1 μg ml^{-1} after 48 h and as much as 87% cell death after 72 h (Fig. 2b). The toxicity of RG-MWCNTs for concentrations of 5–20 μg ml^{-1} appeared to saturate after 48 h whereas for concentrations of 10–20 μg ml^{-1} the toxicity appeared to saturate after 72 h exposure time. It is evident that exposure time plays a significant role in cell viability. Significant decrease in cell viability as the RG-MWCNTs' dose increased from 1 to 5 μg ml^{-1} was observed at 48 h and 72 h (Fig. 2b). At 48 h, the cell viability at lower dosages (1 and 5 μg ml^{-1}) was the same for the two materials and the viability at higher concentrations (10–20 μg ml^{-1}) was similar. At 72 h, substantial decrease in cell viability of MRC-5 cells with concentration was observed for IG-MWCNTs (Fig. 2a). The highest decrease in cell viability of 35% was observed following incubation with 20 μg ml^{-1} of

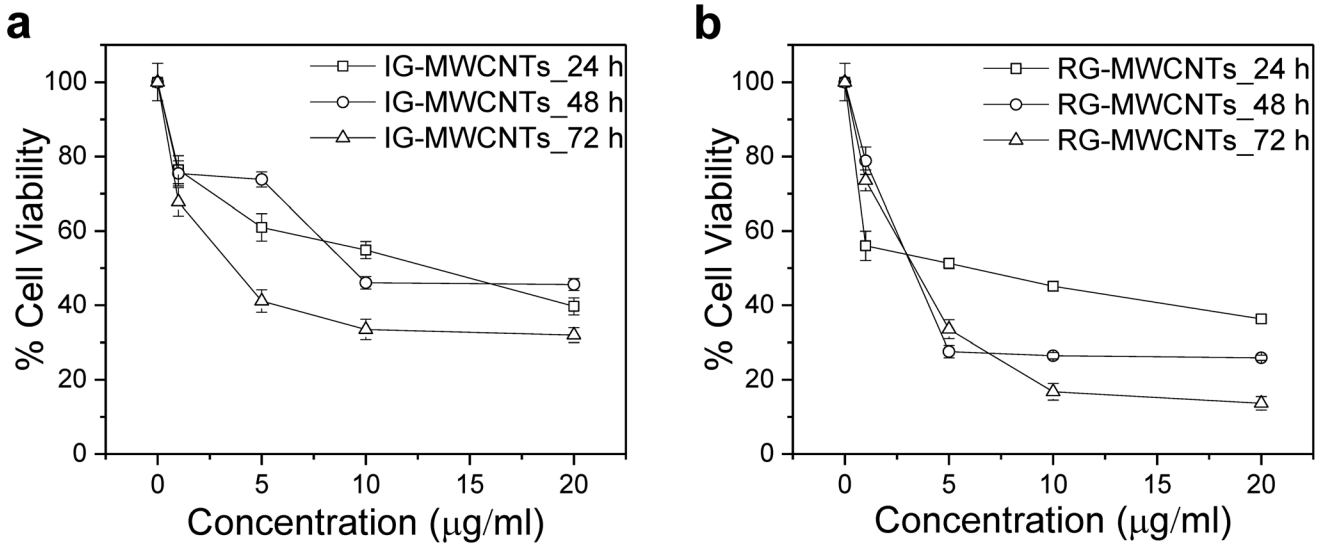

Fig. 2 Toxic effect on the cell viability of MRC-5 cells upon MWCNTs exposure. The effect on MRC-5 cells exposed to varying concentrations of (a) IG-MWCNTs and (b) RG-MWCNTs for 24, 48 and 72 h. Standard error is approximately 5%.

IG-MWCNTs for 72 h whereas the cell viability dropped by 15% upon 72 h exposure to 20 μg ml^{-1} of RG-MWCNTs. Analysis of our data at 95% confidence level, gave $p < 0.0001$* for concentration and time, and $p < 0.0279$ for the type of MWCNT, suggesting dose, exposure time and types of MWCNTs have significant effects on the cellular response. From the above observations, we concluded that RG-MWCNTs exhibited the highest toxicity as compared to IG-MWCNTs after 72 h exposure duration while showed similar toxicity for the 24 h exposure.

Effect of MWCNTs on ROS/RNS generation. Fig. 3a and b clearly show ROS/RNS generation following exposure to MWCNTs in MRC-5 cells. As shown in Fig. 3a, all the three species (oxidative stress, superoxide radicals and NO radicals) were generated in MRC-5 cells following incubation with 20 μg ml^{-1} of either IG-MWCNTs or RG-MWCNTs after 24 h exposure. Non-treated MRC-5 cells displayed both ROS and RNS species, which was further quantified and shown in Fig. 3b. To quantify and confirm our results, we performed total ROS/RNS assay using DCF fluorescence. Total ROS/RNS levels in MRC-5 cells without treatment with either IG-MWCNTs or RG-MWCNTs were normalized to zero % and the change in total ROS/RNS levels following exposure to different concentrations (1 μg ml^{-1} to 20 μg ml^{-1}) of either IG-MWCNT or RG-MWCNTs is shown in Fig. 3b. The decrease in ROS/RNS species amount was observed following exposure to increased concentrations of either IG-MWCNTs or RG-MWCNTs (Fig. 3b). ROS/RNS amounts for cells exposed to 5, 10 and 20 μg ml^{-1} of IG-MWCNTs were lower than non-exposed cells. Surprisingly, the ROS/RNS levels in cells exposed to 20 μg ml^{-1} of RG-MWCNTs were lower than ROS/RNS levels in non-exposed cells. These results imply that at 1 μg ml^{-1}, IG-MWCNTs existed in small nanotube fibers and therefore could efficiently induce ROS/RNS generation. However, at concentrations higher than 5 μg ml^{-1}, IG-MWCNTs formed large agglomerates in cell media causing cell death mainly through a non-oxidative mechanism. In contrast, RG-MWCNTs at concentrations lower than 20 μg ml^{-1} efficiently induced ROS/RNS

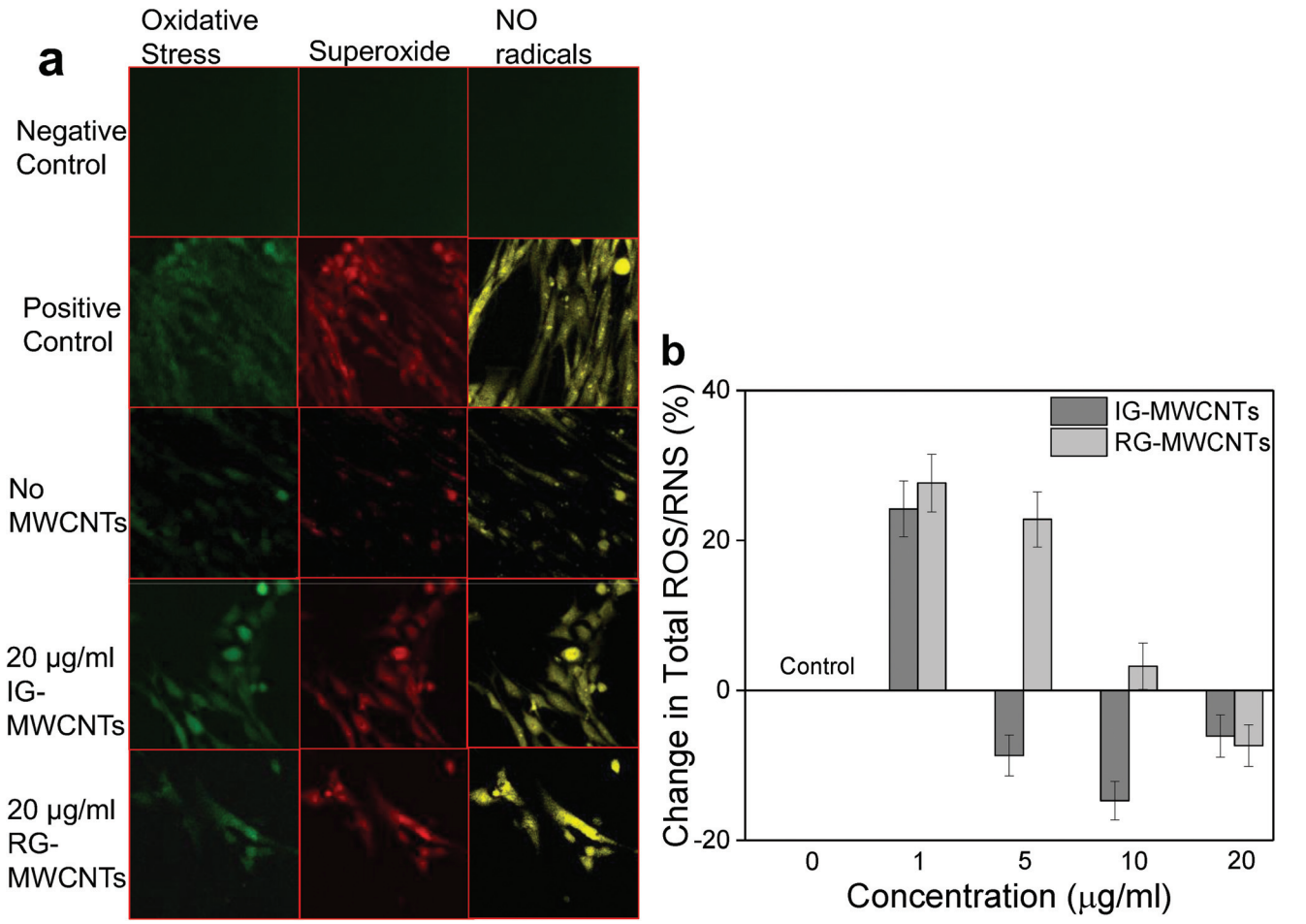

Fig. 3 ROS/RNS generation in MRC-5 cells following MWCNT exposure for 24 h. (a) Confocal fluorescent images of MRC-5 cells showing oxidative stress (green), superoxide radicals (red) and no radicals (yellow). (b) Change in total ROS/RNS following exposure to varying concentrations of MWCNTs with respect to MRC-5 cells non-exposed to MWCNTs (0 μg ml^{-1}). Error bars are standard error of the mean. *$p < 0.001$ *vs.* 0 μg ml^{-1} for both IG-MWCNTs and RG-MWCNTs.

production in MRC-5 cells and caused cell death mainly through the oxidative mechanism. However, 20 μg ml^{-1} of RG-MWCNTs can form larger agglomerates and therefore can induce cell death through cell membrane damage. Thus agglomerate size of MWCNTs determines the toxicity mechanism in MRC-5 cells.

Apoptosis. According to previous studies, cells triggered apoptosis, programmed cell death, as a response to stress induced by carbon nanomaterials. We performed the Hoechst assay and Annexin V assay to determine apoptosis in MRC-5 cells exposed to either IG-MWCNTs or RG-MWCNTs. Fig. 4a illustrates the phase contrast and Hoechst stained images for concentrations of 1 and 20 μg ml^{-1} of IG-MWCNTs or RG-MWCNTs after 24 h. We considered circular evenly stained nuclei as normal (Fig. 4b) and condensed and/or fragmented nuclei as apoptotic cells (Fig. 4c). Apoptotic phenotype was observed for normal cells following exposure to low (1 μg ml^{-1}) or high (20 μg ml^{-1}) concentrations of IG-MWCNTs or RG-MWCNTs (Fig. 4a, right panel). Most of the normal cells died and thereby washed away with PBS following treatment with 1 and 20 μg ml^{-1} of RG-MWCNTs for 24 h. Cells lost their normal elongated shape and appeared more circular as shown in Fig. 4a, left panel. Clumps of cells became more evident for higher concentration of IG-MWCNTs or RG-MWCNTs. The nuclei for these cells showed apoptotic phenotype suggesting both IG-MWCNTs and RG-MWCNTs induced apoptosis. Further, large aggregates of IG-MWCNTs or RG-MWCNTs could be located on the surface of these apoptotic cells. The above results imply the toxicity of both large aggregates and small individual MWCNTs on normal cells. Apoptosis was confirmed using the Annexin V FITC assay, an established fluorescent dye for detecting apoptosis. Increase in concentrations of IG-MWCNTs caused increase in percentage of apoptosis. Lower concentrations (1 and 5 μg ml^{-1}) of RG-MWCNTs caused higher apoptosis as compared to higher concentrations (10 and 20 μg ml^{-1}). Further, large aggregates of IG-MWCNTs or RG-MWCNTs could be located on the surface of these apoptotic cells. The above results imply the toxicity of both large aggregates and small individual MWCNTs on normal cells. The Hoechst assay and Annexin V assay data coincide with our cell viability data providing a further confirmation that normal cells were vulnerable to both MWCNTs.

Imaging MWCNTs in MRC-5 cells using TEM. We confirmed the internalization of MWCNTs inside the MRC-5 cells

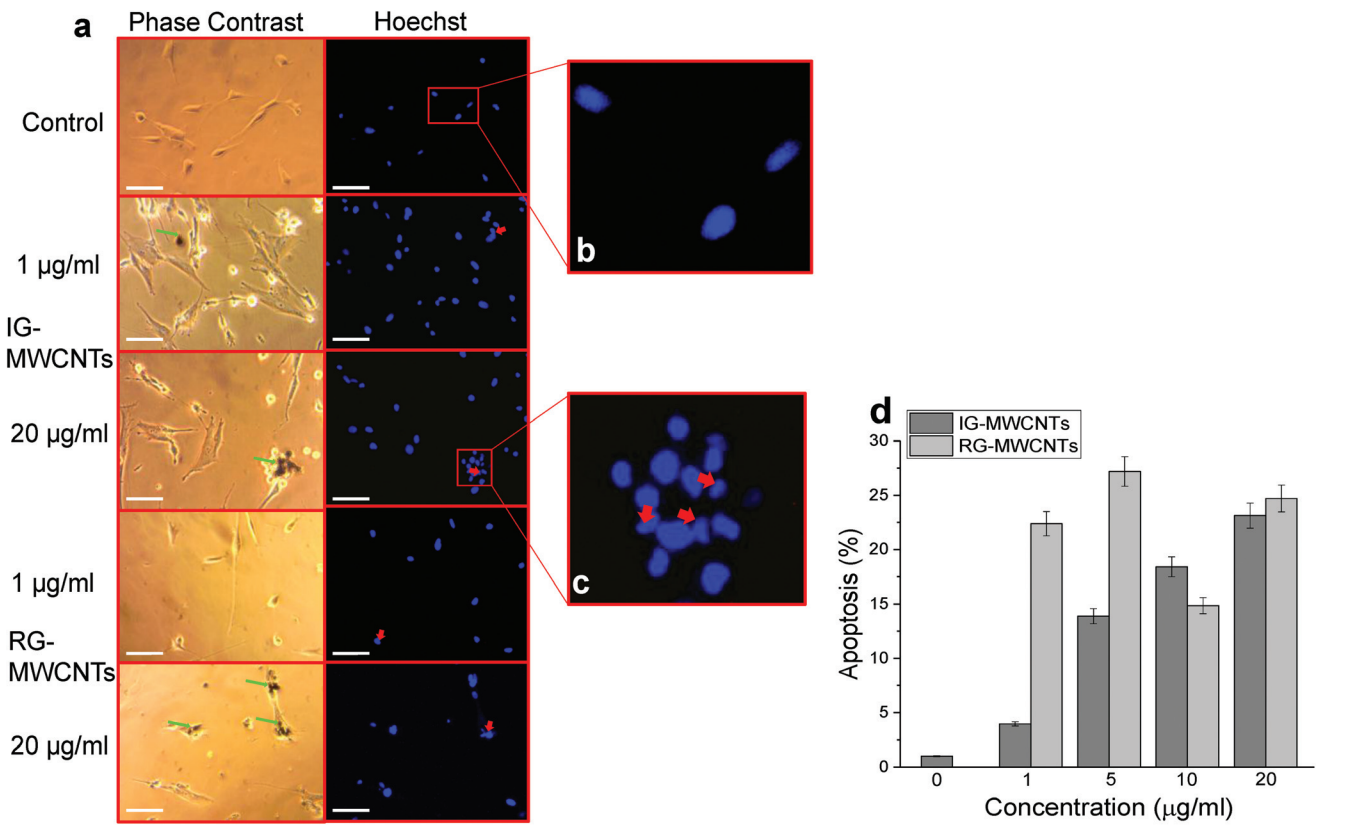

Fig. 4 Apoptosis responses in MRC-5 cells following MWCNTs exposure for 24 h using Hoechst and Annexin V assay. (a) Phase contrast (left panel) images show IG-MWCNTs or RG-MWCNTs (green arrow) and corresponding fluorescent images (right panel) show apoptotic nuclei (red arrow). Scale bar: 5 μm. (b) An enlarged fluorescent image of the selected area from the control showing normal phenotype of MRC-5 nuclei. (c) An enlarged fluorescent image of the selected area from 20 μg ml^{-1} of IG-MWCNTs showing apoptotic phenotype of MRC-5 nuclei. (d) Percentage of apoptosis following exposure to varying concentrations of MWCNTs with respect to MRC-5 cells non-exposed to MWCNTs (0 μg ml^{-1}). Error bars are standard error of the mean. *$p < 0.001$ *vs.* 0 μg ml^{-1} for both IG-MWCNTs and RG-MWCNTs.

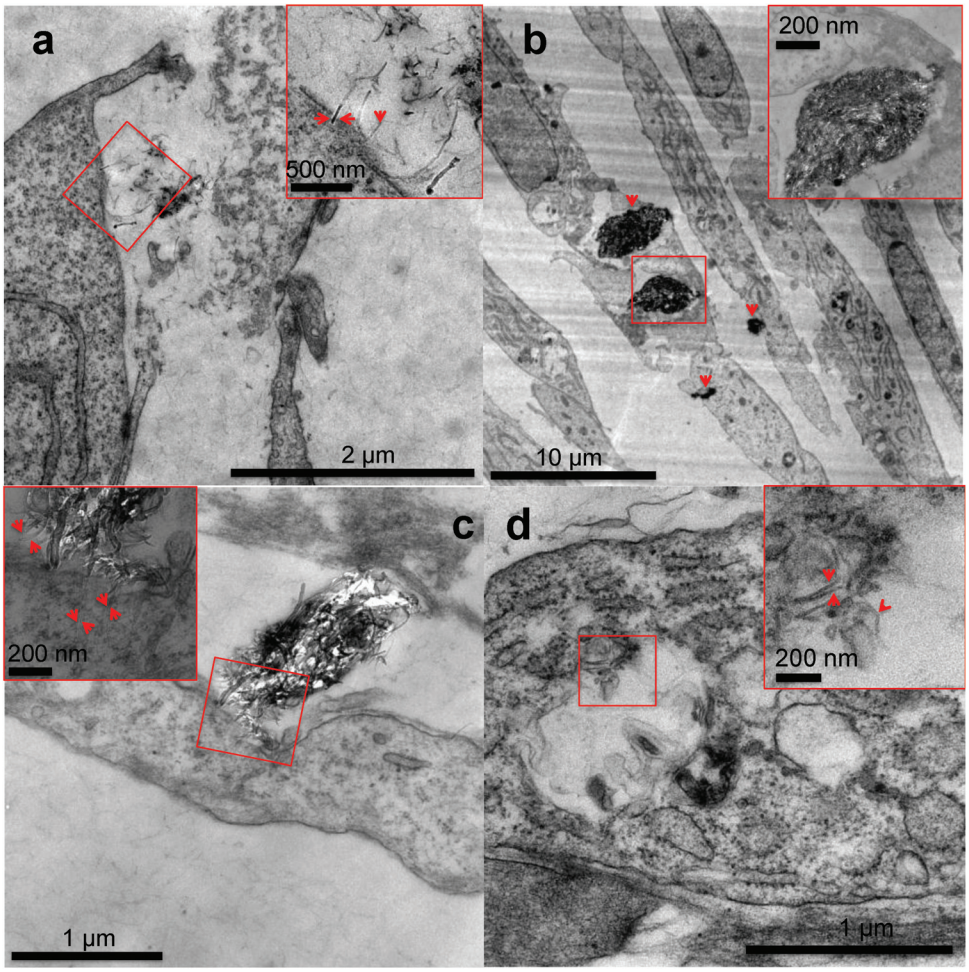

Fig. 5 Transmission electron microscopy analysis of MRC-5 cells cultured for 24 h in cell culture medium conditioned with IG-MWCNTs or RG-MWCNTs. (a) Single RG-MWCNTs existing in the microenvironment of MRC-5 cells. Arrows in the enlarged higher magnification image of the selected area show individual RG-MWCNTs entering MRC-5 through the membrane. (b) Large denser agglomerates of IG-MWCNTs entering cells as well as exiting inside cells thereby causing damage to the entire cell. Arrows show agglomerates. An enlarged higher magnification image of the selected area confirms agglomerates of nanotubes. (c) Interaction of large agglomerates of RG-MWCNTs with the cell membrane of MRC-5 cells. An enlarged high magnification image of the selected area displays single nanotubes dangling from large agglomerate embedded in the cell membrane causing membrane damage. Arrows indicate single nanotubes clearly present inside the cell membrane. (d) Individual RG-MWCNTs internalized by MRC-5 cells in vesicles. An enlarged high magnification image of the selected area shows individual separated short nanotubes. Arrows indicate single RG-MWCNTs.

using transmission electron microscopy. Fig. 5 illustrates the TEM micrographs obtained after incubation of MRC-5 cells with 20 μg ml^{-1} of IG-MWCNTs or RG-MWCNTs. As shown in Fig. 5a individual short nanotubes of RG-MWCNTs (≤100 nm) can efficiently enter into the cell membrane. These nanotubes can cause extensive disruption of the cell membrane and cell damage. In contrast, large dense agglomerates of IG-MWCNTs were taken up by the cell which caused change in morphology of MRC-5 cells. Agglomerates of RG-MWCNTs appeared less dense as compared to agglomerates of IG-MWCNTs. Further, individual nanotubes dangling from these agglomerates could efficiently interact with the cell membrane and were found to be embedded inside the membrane. Individual short RG-MWCNTs were efficiently internalized by MRC-5 cells (Fig. 5d). The above results confirm the efficient interaction and internalization of both agglomerates and individual MWCNTs inside the MRC-5 cells.

Discussion

In this study, we compared the cell response of fetal lung fibroblasts (MRC-5) following exposure to different types of MWCNTs having different chemical impurities. We elucidate how the cell response varies with chemical composition and the size of MWCNTs' agglomerates and length of MWCNTs between types of MWCNTs. We do not use the centrifugation method to purify MWCNTs or purified MWCNTs for this study because we wanted to study the occupational exposure to the airborne CNTs released from the raw CNTs. Further, we did

not use surfactants to disperse the MWCNTs in water. We wanted to investigate toxicity caused by MWCNTs without surface modification or any property changes. The original material without surface purification or modification was needed for this goal. We were successful to obtain dispersion of CNTs in water for 10 minutes sonication without using a surfactant. We observed significant differences in the toxicity response of fetal lung fibroblasts (MRC-5) exposed to MWCNTs used in this study. Both IG-MWCNTs and RG-MWCNTs cause decrease in cell viability of MRC-5 cells following exposure for 24 h. Toxicity for both IG-MWCNTs and RG-MWCNTs could be exclusively due to their flexible rod structure. Rod-shaped CNTs can easily enter the cells with the long axis of cylindrical nanotubes interacting with the cell membrane because of its extensive binding with surface receptors.[18] Since MWCNTs have a high surface to volume ratio, they can interact with the cell membrane and are readily taken up inside the cell, which increases their probability to induce toxicity by interacting with cellular organelles such as the nucleus, mitochondria, endoplasmic reticulum *etc*.

Additionally, RG-MWCNTs were found to be more toxic than IG-MWCNTs. This was mainly due to small size/shorter fiber of RG-MWCNTs, which were broken into smaller nanotubes (size <100 nm) and were uniformly suspended in distilled water following sonication. Chemical impurities and different functional groups made the surface of IG-MWCNTs highly hydrophobic. IG-MWCNTs could have hydrophobic alkyl groups on their surface that cause them to bundle up into multiple tubes and increased their overall length.[21] The difference in size of RG-MWCNT and IG-MWCNT agglomerates found in this study was likely due to the presence of different functional groups (carbonyl and carboxyl) and the presence of metals (impurities), which affected the interaction of MWCNTs with cell medium. Since nanotubes shorter than 100 nm are highly favored for cell uptake, the short nanotubes of RG-MWCNTs can insert into lipid bilayers and live cell membranes to attain transmembrane protein configuration (channels) that are capable of performing exchange of materials from the cells. They can easily extract large volume of phospholipids from the cellular membrane impelled by van der Waal's force. The presence of MoS_2 also contributed to the RG-MWCNTs toxicity. Molybdenum metal and compounds, especially MoS_2, have been associated with acute and chronic toxicity.[22]

RG-MWCNTs exhibited higher intensity of a carbonyl peak than IG-MWCNTs (Fig. S2b†). The carbonyl group in MWCNTs arises from ketones and quinones that are associated with basal carbonyl groups. The toxicity of both IG-MWCNTs and RG-MWCNTs can be associated with the presence of carbonyl groups in the structure, which can interact with the amine group of cellular proteins and form amides and esters. Cellular interactions have been established between cells' protein amine groups and free C═O groups of chemicals contributing to the cellular response.[23] RG-MWCNTs are capable of interacting with proteins inside the cell, leading to harmful effects. Even though short-term exposure to RG-MWCNTs induced higher toxicity in MRC-5 cells, IG-MWCNTs long-term exposure caused higher fatality. This could be due to the accumulation of tangled IG-MWCNTs inside the cells overtime in contrast to short RG-MWCNTs that could be excreted by cells easily.

CNT mediated cytotoxicity is mainly due to oxidative stress, genotoxicity and apoptosis.[24,25] It is known that CNTs cause imbalance between the generation of free radicals and antioxidant defenses. Exposure to 1 μg ml^{-1} of either IG-MWCNTs or RG-MWCNTs for 24 h caused an increase in the amount of ROS/RNS whereas exposure to 20 μg ml^{-1} of MWCNTs reduced the production of these species. The above result can be explained through the possibility that 1 μg ml^{-1} of MWCNTs was uniformly suspended in the cell medium and therefore could efficiently induce cell oxidative stress. Large MWCNT agglomerates might have formed when suspended at concentrations above 5 μg ml^{-1}, and therefore very few individual nanotubes could actually enter the cells. At concentrations below 20 μg ml^{-1}, RG-MWCNTs induce cell death through an oxidative stress mechanism while at 20 μg ml^{-1} the mechanism shifts to other non-oxidative processes like cell membrane disruption (necrosis). However, the threshold for IG-MWCNTs to cause cell death through non-oxidative processes is above 5 μg ml^{-1}. Thus, IG-MWCNTs mainly induce toxicity through non-oxidative processes whereas RG-MWCNTs caused cell death mainly through oxidative mechanisms. Some researchers have suggested that there is a strong relationship between induction of programmed cell death and oxidative damage following exposure to CNTs.[26,27] The effect of ROS/RNS production leading to apoptosis can be seen in Fig. 4. We observed fragmented and condensed nuclei for cells exposed to all concentrations of both IG-MWCNTs and RG-MWCNTs, which are the features of apoptotic nuclei. Moreover, from Annexin V assay, we confirmed that all concentrations of both IG-MWCNTs and RG-MWCNTs induce apoptosis. But exposure of MRC-5 cells to low concentrations (1 and 5 μg ml^{-1}) of RG-MWCNTs resulted in higher percentage of apoptotic cells than exposure to lower concentrations (1 and 5 μg ml^{-1}) of IG-MWCNTs. Further, there were very few cells found adhered to the tissue plate following exposure to RG-MWCNTs, which had apoptotic nuclei and an irregular shape. On the contrary, cells remained adhered to the surface after exposure to IG-MWCNTs and had elongated shape with a disrupted cell membrane. These observations imply that all concentrations of RG-MWCNTs cause cell death through oxidative stress mediated apoptosis. For RG-MWCNTs, the shorter nanotubes (<100 nm) are able to efficiently interact with the cell membrane and enter the cell. These induce production of free radicals in mitochondria and cause programmed cell death. For MRC-5 cells exposed to IG-MWCNTs, internalization of large dense agglomerates may have resulted in cell membrane damage and thereby cell death. Lower ROS/RNS levels at high concentrations of IG-MWCNTs and RG-MWCNTs exposure hint at other pathways that triggered cell death. Both individual and agglomerates of MWCNTs can extensively interact with the cells and induce toxicity. From the above results, we are

able to conclude that the chemical impurities in MWCNTs can affect agglomeration and therefore contribute to different toxicity in human lung cells. As shown in our study, MWCNT toxicity is strongly affected by size and chemical impurities along with concentration and time. It is important to understand the purity of the materials and the presence of trace amounts of other elements including catalysts, which could contribute to harmful effects in the cell.

Conclusions

In our study, we have shown that MWCNTs containing MoS_2 contamination may cause higher toxicity as compared to MWCNTs containing only Mo. Also presence of MoS_2, along with other surface properties, may affect the dispersibility of MWCNTs in water, which could further affect the toxicity mechanism. Results indicate that MWCNTs used in this study were extensively toxic to normal lung cells and the possible mechanisms could be through oxidative damage and cell membrane integrity disruption dependent on MWCNTs agglomeration and chemical impurities. Furthermore, we have shown that low concentrations (1 μg ml^{-1}) of MWCNTs could potentially be very toxic to human fetal lung fibroblasts after a short (24 h) exposure period. Both agglomerates and individual MWCNTs can enter the fetal fibroblasts and are taken up efficiently by cells. Through TEM imaging, this is the first time short individual non-functionalized MWCNTs have been clearly visualized inside the fetal lung fibroblasts (MRC-5). Altogether, MWCNT toxicity is greatly dependent on physiochemical properties and therefore it would be unwise to group all MWCNTs together in terms of their toxicity. Since nanomaterials are extensively useful in different fields, their detailed characterization is important when studying their impact on human health, allowing their use for human progress.

Acknowledgements

Authors thank Christopher J. Gilpin for technical support on TEM and EDX analysis. Authors also thank Laurie M. Mueller for preparation of grids for cell samples used for TEM analysis. The authors declare no conflict of interest relating to the material presented in this article. Its contents, including any opinions and/or conclusions expressed, are those of the authors. This research was partially supported by School of Health Sciences, College of Health and Human Science at Purdue University.

References

1 S. Iijima and I. Toshinari, Single-shell of Carbon Nanotubes of 1-nm Diameter, *Nature*, 1993, 363.
2 F. Piccinno, F. Gottschalk, S. Stefan and B. Nowack, Industrial Production Quantities and Uses of ten Engineered Nanomaterials in Europe and the World, *J. Nanopart. Res.*, 2012, 14.
3 M. Kumar and Y. Ando, Chemical Vapor Deposition of Carbon Nanotubes: A Review on Growth Mechanism and Mass Production, *J. Nanosci. Nanotechnol.*, 2010, **10**, 3739–3758.
4 Global Carbon Nanotubes Market – Industry Beckons 2011.
5 A. P. Parish, in *Production and Application of Carbon Nanotubes, Carbon Nanofibers, Fullerenes, Graphene and Nanodiamonds: A Global Technology Survey and Market*, Innovative Research and Products, Inc., 2011, p. 531.
6 P. Ball, Roll up for the revolution, *Nature*, 2001, **414**, 142–144.
7 A. Pistone, D. Iannazzo, S. Panseri, M. Montesi, A. Tampieri and S. Galvagno, Hydroxyapatite-Magnetite-MWCNT Nanocomposite as a Biocompatible Multifunctional Drug Delivery System for Bone Tissue Engineering, *Nanotechnology*, 2014, **25**, 425701.
8 H. T. Zhang, P. Pan, M. R. Wang, Z.-C. Yang, J. L. Liu and Z. Wei, Enhanced Optical Limiting of Dispersible MWCNTs/TiO2 Nanocomposite, *Opt. Laser Technol.*, 2015, **67**, 44–49.
9 J. Du, S. Wang, H. You and X. Zhao, Understanding the Toxicity of Carbon Nanotubes in the Environment is Crucial to the Control of Nanomaterials in Producing and Processing and the Assessment of Health Risk for Human: a review, *Environ. Toxicol. Pharmacol.*, 2013, **36**, 451–462.
10 J. M. Hillegass, A. Shukla, S. A. Lathrop, M. B. MacPherson, N. K. Fukagawa and B. T. Mossman, Assessing Nanotoxicity in Cells In Vitro, *Wiley Interdiscip. Rev.: Nanomed. Nanobiotechnol.*, 2010, **2**, 219–231.
11 C. L. Ursini, D. Cavallo, A. M. Fresegna, A. Ciervo, R. Maiello, G. Buresti, S. Casciardi, F. Tombolini, S. Bellucci and S. Iavicoli, Comparative Cyto-genotoxicity Assessment of Functionalized and Pristine Multiwalled Carbon Nanotubes on Human Lung Epithelial Cells, *Toxicol. In Vitro*, 2012, **26**, 831–840.
12 D. Cui, F. Tian, C. S. Ozkan, M. Wang and H. Gao, Effect of Single Wall Carbon Nanotubes on Human HEK293 Cells, *Toxicol. Lett.*, 2005, **155**, 73–85.
13 G. Jia, H. Wang, L. Yan, X. Wang, R. Pei, T. Yan, Y. A. Zhao and X. Guo, Cytotoxicity of Carbon Nanomaterials: Single-Wall Nanotube, Multi-Wall Nanotube, and Fullerene, *Environ. Sci. Technol.*, 2005, **39**, 1378–1383.
14 F. Tian, D. Cui, H. Schwarz, G. G. Estrada and H. Kobayashi, Cytotoxicity of Single-Wall Sarbon Nanotubes on Human Fibroblasts, *Toxicol. in Vitro*, 2006, **20**, 1202–1212.
15 K. Pulskamp, S. Diabate and H. F. Krug, Carbon Nanotubes Show No Sign of Acute Toxicity But Induce Intracellular Reactive Oxygen Species in Dependence on Contaminants, *Toxicol. Lett.*, 2007, **168**, 58–74.
16 J. Meng, X. Cheng, J. Liu, W. Zhang, X. Li, H. Kong and H. Xu, Effects of Long and Short Carboxylated or Aminated Multi-Walled Carbon Nanotubes on Blood Coagulation, *PLoS One*, 2012, **7**, e38995.

17 A. Fraczek-Szczypta, E. Menaszek, T. B. Syeda, A. Misra, M. Alavijeh, J. Adu and S. Blazewicz, Effect of MWCNT Surface and Chemical Modification on In Vitro Cellular Response, *J. Nanopart. Res.*, 2012, **14**, 1181.

18 N. Gao, Q. Zhang, Q. Mu, Y. Bai, L. Li, H. Zhou, E. R. Butch, T. B. Powell, S. E. Snyder, G. Jiang and B. Yan, Steering Carbon Nanotubes to Scavenger Receptor Recognition by Nanotube Surface Chemistry Modification Partially Alleviates NFκB Activation and Reduces Its Immunotoxicity, *ACS Nano*, 2011, **5**, 4581–4591.

19 A. Fraczek, E. Menaszek, C. Paluszkiewicz and M. Blazewicz, Comparative In Vivo Biocompatibility Study of Single- and Multi-Wall Carbon Nanotubes, *Acta Biomater.*, 2008, **4**, 1593–1602.

20 J. Cheng and S. H. Cheng, Influence of Carbon Nanotube Length on Toxicity to Zebrafish Embryos, *Int. J. Nanomed.*, 2012, **7**, 3731–3739.

21 H. Ali-Boucetta, A. Nunes, R. Sainz, M. A. Herrero, B. Tian, M. Prato, A. Bianco and K. Kostarelos, Asbestos-like Pathogenicity of Long Carbon Nanotubes Alleviated by Chemical Functionalization, *Angew., Chem., Int. Ed.*, 2013, **52**, 2274–2278.

22 E. L. Chng, Z. Sofer and M. Pumera, MoS_2 Exhibits Stronger Toxicity with Increased Exfoliation, *Nanoscale*, 2014, **6**, 14412–14418.

23 S. I. Han, B. S. Kim, S. W. Kang, H. Shirai and S. S. Im, Cellular Interactions and Degradation of Aliphatic Poly(ester amide)s Derived from Glycine and/or 4-amino butyric acid, *Biomaterials*, 2003, **24**, 3453–3462.

24 J. Boczkowski and S. Lanone, Respiratory Toxicities of Nanomaterials - A Focus on Carbon Nanotubes, *Adv. Drug Delivery Rev.*, 2012, **64**, 1694–1699.

25 A. A. Shvedova, A. Pietroiusti, B. Fadeel and V. E. Kagan, Mechanisms of Carbon Nanotube-Induced Toxicity: Focus on Oxidative Stress, *Toxicol. Appl. Pharmacol.*, 2012, **261**, 121–133.

26 A. A. Shvedova, E. R. Kisin, A. R. Murray, O. Gorelik, S. Arepalli, V. Castranova, S. H. Young, F. Gao, Y. Y. Tyurina, T. D. Oury and V. E. Kagan, Vitamin E Deficiency Enhances Pulmonary Inflammatory Response and Oxidative Stress Induced by Single-Walled Carbon Nanotubes in C57BL/6 Mice, *Toxicol. Appl. Pharmacol.*, 2007, **221**, 339–348.

27 Y. Y. Tyurina, E. R. Kisin, A. Murray, V. A. Tyurin, V. I. Kapralova, L. J. Sparvero, A. A. Amoscato, A. K. Samhan-Arias, L. Swedin, R. Lahesmaa, B. Fadeel, A. A. Shvedova and V. E. Kagan, Global Phospholipidomics Analysis Reveals Selective Pulmonary Peroxidation Profiles upon Inhalation of Single-Walled Carbon Nanotubes, *ACS Nano*, 2011, **5**, 7342–7353.

